A Cellular Automaton Model for the Regulatory Behavior of Muscle Thin Filaments

Guangzhou Zou* and George N. Phillips, Jr.‡

*Department of Computer Science and ‡Department of Biochemistry and Cell Biology, W. M. Keck Center for Computational Biology, Rice University, Houston, Texas 77251-1892 USA

ABSTRACT   Regulation of skeletal muscle contraction is achieved through the interaction of six different proteins: actin, myosin, tropomyosin, and troponins C, I, and T. Many experiments have been performed on the interactions of these proteins, but comparatively less effort has been spent on attempts to integrate the results into a coherent description of the system as a whole. In this paper, we present a new way of approaching the integration problem by using a cellular automaton. We assign rate constants for state changes within each constituent molecule of the muscle thin filament as functions of the states of its neighboring molecules. The automaton shows how the interactions among constituent molecules give rise to the overall regulatory behavior of thin filaments as observed in vitro and is extendable to in vivo measurements. The model is used to predict myosin binding and ATPase activity, and the result is compared with various experimental data. Two important aspects of regulation are revealed by the requirement that the model fit the experimental data: (1) strong interactions must exist between two successively bound myosin heads, and (2) the cooperative binding of calcium to the thin filament can be attributed in a simple way to the interaction between neighboring troponin-tropomyosin units.

INTRODUCTION

To understand the behavior of complex systems, it is essential to see how behavior of simple constituent systems are coupled. A class of the simplest behaviors can be formally described by a set of abstract computational machines called *finite automata* (Brookshear, 1989). A finite automaton is an entity that consists of a finite set of states and undergoes discrete state changes according to a finite set of rules. A large number of finite automata can be combined together. Thus, each finite automaton is a single "cell" of the integrated system. The state transition of each automaton is determined by the states of its neighboring automata. A simple version of such integrated systems is known as *cellular automata* (Wolfram, 1984). A typical cellular automaton consists of a regular uniform lattice (cellular space) with a discrete variable at each lattice site (i.e., each site is a finite automaton) (Wolfram, 1984; Kauffman, 1969). The cellular space could be one-, two-, or three-dimensional. Every site in the cellular space is allowed to interact with sites in its neighborhood. The interaction of a site with its neighbors is specified through the cellular automaton rule that consists of a complete set of local rules. Mathematically, a cellular automaton rule is a map that relates a site's neighborhood-configuration at time t to the site's state at time $t + 1$. When we apply a cellular automaton rule to every site in a defined cellular space simultaneously, the simple behaviors of all these finite automata are coupled together in the time dimension. As a consequence, higher level behaviors can emerge spontaneously.

In this study, we simulate the behavior of individual molecules of muscle thin filaments during their regulation from the relaxed, or "off" state, to the contracting, or "on" state. A one-dimensional array of finite automata is defined based only on local interactions. The overall regulatory behavior of muscle thin filaments emerges from the collective behavior of these finite automata.

The key assumption in this paper is that the state-transition rate constant of each constituent molecule of the thin filament is a function of the states of its neighboring molecules. Traditionally, the kinetics of the conformational change of a protein is approximated by

$$-\frac{d[X]}{dt} = k[X] - k'[X'],$$

where X and X' are two different conformations of a protein, and $[X]$ and $[X']$ are the corresponding concentrations. Parameters k and k' are transition rate constants. The mechanism can also be simply denoted as

$$X \underset{k'}{\overset{k}{\rightleftharpoons}} X'.$$
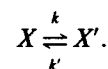
The transition rate constant k, however, only provides an average description of the behavior of a large number of molecules. When we concentrate on the behavior of an individual molecule, especially in a system where molecules are bound to each other, the exact transition rate constant of the molecule would more likely depend on the states of its neighboring molecules (the neighborhood-configuration), i.e.,

$$k = \begin{cases} k_1 & \text{for neighborhood-configuration 1} \\ k_2 & \text{for neighborhood-configuration 2} \\ \vdots \\ k_n & \text{for neighborhood-configuration } n. \end{cases} \quad (1)$$

Cellular automata provide a framework in which we can implement the above assumptions and see the logical consequence of the interdependencies. The value of the transition rate constants versus the neighborhood-configurations of a molecule corresponds to the local transition rules of cellular automata. In this study, the transition rules for the constituent molecules of the muscle thin filament are constructed based on an understanding of the structure of the thin filament and experimental kinetic data on the local interactions between the molecules.

Our goal is to build a computational machine that can mimic muscle filaments under a wide variety of experimental conditions rather than to propose a new data-fitting technique that can simply reproduce data curves. The transition rate constants in our model are fundamentally different from simple data-fitting parameters in the following ways: (1) the transition rate constants have clear physical meaning and correspond to well defined chemical processes; (2) the transition rate constants can be independently measured, in principle, without referring to any specific model; and (3) once the values of the rate constants are determined, either by direct experiment or by comparisons of the model with certain data sets, they are not allowed to have multiple values for comparison with different experimental data. In this paper, we determine six binding rate constants of myosin to actin from myosin binding data, and none of them are changed in the subsequent comparisons with experimental results of ATPase, pCa, or dynamics. As we will demonstrate later, additional insight about the protein interactions required for muscle regulation can be obtained by comparing the transition rate constants corresponding to different neighborhood-configurations.

The paper is organized as follows. First, we construct a cellular automaton that represents the regulatory aspects of the muscle thin filament. Then, we fit the the equilibrium and steady-state behavior of the cellular automaton to various in vitro experimental data including binding of myosin S1 to actin and the binding of Ca^{2+} to troponin. These comparisons define the association rate constants of myosin binding to actin and calcium to troponin. Next, we compare the predictions of this model with the experimental data on ATPase activity. Finally, we discuss the implications of the results and suggest how the model could be extended to study the behavior of intact muscle fibers.

MODEL CONSTRUCTION

A cellular automaton is defined by two elements: (i) the cellular space and the number of states for each site in the cellular space; and (ii) the transition rules of the states (the cellular automaton rule). In this section, we define a formal cellular space and outline a set of transition rules that specifies the behavior of the constituent molecules of the thin filament. A formal description of the transition rules is given in the Appendix.

The structure of muscle

The basic functional and structural unit of muscle, the sarcomere, contains two kinds of filaments. The thin filament consists mainly of actin, tropomyosin, and troponin. Actin monomers are arranged in a long helical polymer known as F-actin. The F-actin helix may be regarded as either a two-stranded structure with a half-pitch of about 37 nm or a single-stranded genetic helix with a pitch of about 5.9 nm. A tropomyosin molecule is about 41 nm long. Tropomyosin molecules form head-to-tail connections and bind to actin, running along the long-pitch helical strands of F-actin. Troponin molecules are bound to each tropomyosin molecule every 38 nm along F-actin. There exists a stoichiometry of seven actin molecules to one tropomyosin and one troponin (Fig. 1). The troponin molecule has a complex structure consisting of three subunits, in which the troponin subunit C (TnC) is a Ca^{2+}-binding protein. The thick filament consists mainly of the protein myosin. A subfragment of myosin called "S1" or the myosin "head" carries the actin-binding site and ATP hydrolysis site. The interaction between S1 and actin sites causes the contraction of the muscle and force production. The interaction between S1 and actin is usually described by a cross-bridge model that includes cyclic attachment and detachment of heads while hydrolyzing ATP (Lymn and Taylor, 1971; see also reviews by Rayment and Holden, 1993; Hibberd and Trentham, 1986). The regulation of muscle contraction has been discussed in terms of several models (Hill et al., 1980; Hill, 1983; Brandt et al., 1980, 1982; McKillop and Geeves, 1991; Tobacman and Adelstein, 1986; Phillips et al., 1986; Williams et al., 1988), all with the common feature that there is strong cooperative behavior between the various components (see review by Chalovich, 1992).

Assumptions of the model

In our model, we assume that each actin site on the thin filament has two possible states: an active state (analogous to strongly bound myosin) and an inactive state (weakly bound myosin or no myosin bound) (Fig. 2 a). The active
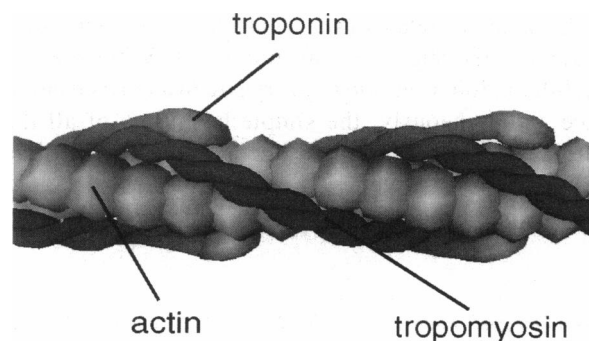

FIGURE 1 Simplified illustration of the thin filament showing the stoichiometry of seven actin sites to one tropomyosin and one troponin on the muscle thin filament.

state of an actin site corresponds to the binding of myosin subfragment 1 (S1) in a particular way that results in an enzymatically active complex. An actin site contributes to ATP hydrolysis and force generation only when it enters the active state.

We assume that each troponin molecule can also be in one of two possible states, an inhibiting state and a facilitating state, and we consider each tropomyosin-troponin complex an integrated functional unit (Tm-Tn unit). The two states of troponin molecule correspond to two conformations of the Tm-Tn unit (Fig. 2, a and b). A Tm-Tn unit in the inhibiting state inhibits the activation of nearby actin sites, whereas a Tm-Tn unit in the facilitating states facilitates the activation of nearby actin sites.
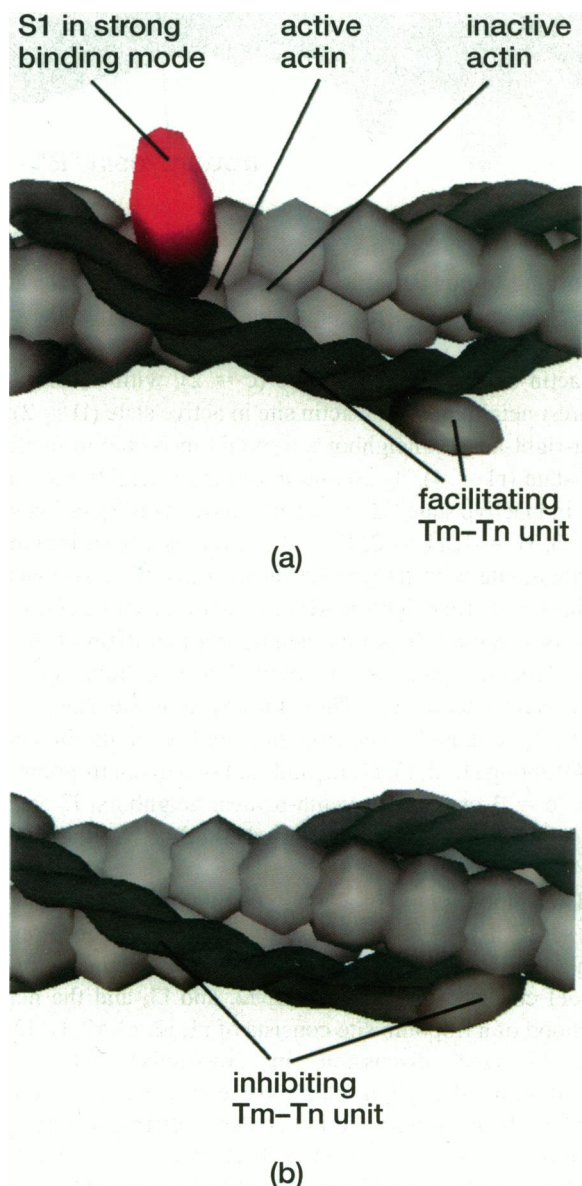

FIGURE 2   Graphical illustration of the states of the model. The sizes of some components are exaggerated for illustrative purposes.

We further assume that, as the result of the interaction, the state transition rate constant of any given actin site or Tm-Tn unit is a function of the state of the neighboring actin sites and Tm-Tn units.

Possible cooperative interactions of actin sites on the thin filament could exist both along the long-pitch actin strands and/or between the actin strands (DasGupta and Reisler, 1992). There is no compelling evidence, however, that the cooperativity between the strands exists and contributes significantly to the regulatory behavior of the thin filament. We assume, therefore, that the cooperativities of actin sites on the thin filament are mainly one-dimensional and are expressed along the long strands of the thin filament primarily by tropomyosin molecules. The model would be adapted to include interstrand effects by going to a two- or three-dimensional automaton in future versions if it were deemed to be appropriate.

In the following section, we will map the thin filament onto a one-dimensional array of finite automata (the cellular space). The transition rate constant of an actin or Tm-Tn unit, which gives the state-transition probability of the corresponding automaton, is determined by the states of the neighboring automata (the transition rules).

Cellular space and transition rules of the model

We let a finite one-dimensional lattice (a one-dimensional cellular space) represent one long-pitch actin strand of a muscle thin filament. We let each lattice site (a finite automaton) represent an actin monomer or a troponin molecule. We assume that there is a troponin molecule for every seven actin sites. The tropomyosin position on each actin monomer is determined by the state of the nearest troponin molecule.

We let the inactive state of an actin site be state 1, denoted by s_1, and it is represented by a green lattice site in the cellular space (Fig. 3). The active state of an actin site is defined as state 2, denoted by s_2, and is represented by a red lattice site in the cellular space (Fig. 3). The inhibiting state of a troponin will be state 3, denoted by s_3, and will be represented by a black lattice site in the cellular space (Fig. 3). This troponin state also corresponds to a particular conformation (or position) of the Tm-Tn unit (Fig. 2 b). We let the facilitating state of troponin be state 4, denoted by s_4, and it is represented by a yellow lattice site in the cellular space (Fig. 3). This troponin state corresponds to the second conformation of Tm-Tn unit (Fig. 2 a).
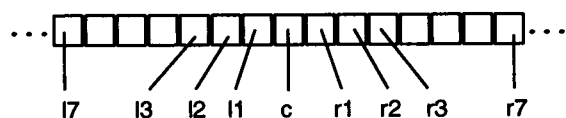
In Fig. 3, the lattice site occupied by a troponin molecule is also an actin site, but it has a very small chance of being activated because of the interference of the head of troponin molecule. The portion of the cellular space in Fig. 3 corresponds to a certain configuration of a thin filament section along one strand of actin-tropomyosin, labeled "A" in Fig. 3. (The configuration along the strand "B" in Fig. 3 and other thin filaments would be determined by the other portions of the cellular space not shown in Fig. 3).

FIGURE 3 Correspondence between the one-dimensional cellular space and the long-pitch strand of the thin filament. The cellular space of our model is defined as a one-dimensional lattice with each lattice site in one of the states specified in the model. The portion of cellular space shown here is in an exact correspondence to a section of the muscle thin filament along the tropomyosin "A" in the figure. Note that the dynamics of a long-pitch strand of the thin filament corresponds to the one-dimensional cellular automaton.
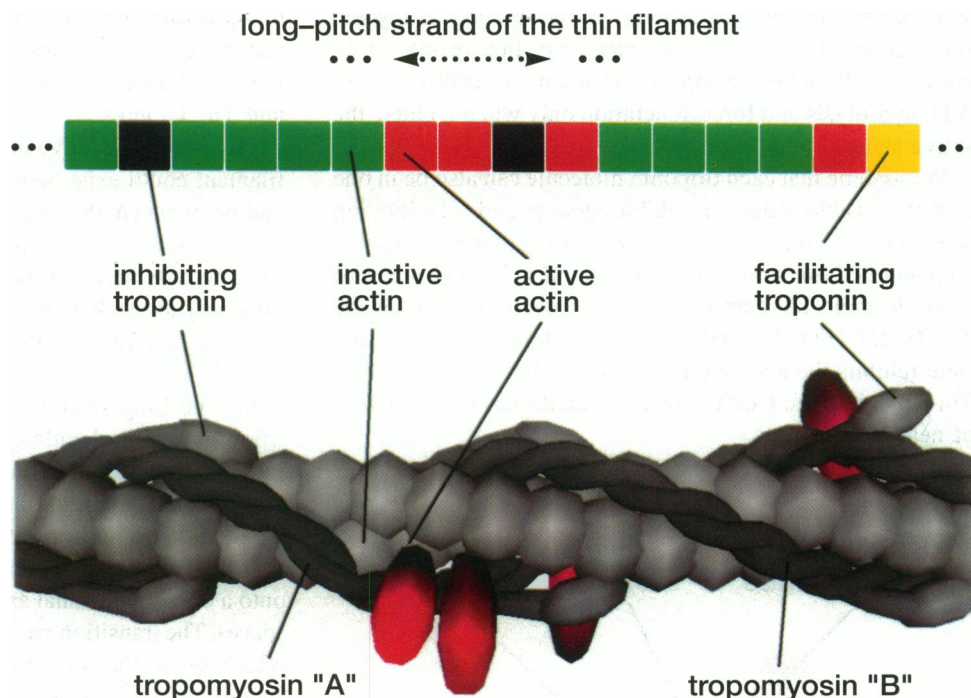
Two adjacent lattice sites in the cellular space are called first-nearest neighbors. If two sites are separated by a distance of one lattice site, then they are the second-nearest neighbors. If two lattice sites are separated by a distance of two sites, then they are the third-nearest neighbors, and so on. In one-dimensional cellular space, every lattice site has two first-nearest neighbors, one on the right and one on the left. Similarly, in one-dimensional cellular space, every lattice site has two second-nearest neighbors, two third-nearest neighbors, etc.

For any given site denoted as c in the cellular space, we let $r1$, $r2$, $r3$, and $r7$ be the current states of its first-, second-, third-, and seventh-right-nearest neighbors, respectively, and let $l1$, $l2$, $l3$, and $l7$ be the current states of its first-, second-, third-, and seventh-left-nearest neighbors, respectively (Fig. 4). Notice that c and its neighbors $r1$, $r2$, $r3$, $r7$,

$l1$, $l2$, $l3$, and $l7$ can be either actin or troponin sites, and according to our definition, can take value 1 or 2 for actin sites, and 3 or 4 for troponin sites. For example, the configuration with $c = 2$, $l1 = 2$, $r1 = 4$, $l2 = 1$ . . . represents an actin site in the active state ($c = 2$), with its first-left-nearest neighbor also an actin site in active state ($l1 = 2$), its first-right-nearest neighbor a troponin molecule in facilitating state ($r1 = 4$), its second left-nearest neighbor an actin site in inactive state ($l2 = 1$). Similarly, a configuration with $c = 3$, $l1 = 1$, $r1 = 2$, $l7 = 4$ . . . represents an inhibiting troponin site with its first-left-nearest neighbor an inactive actin site, its first-right-nearest neighbor an active actin site, and its seventh-left-nearest neighbor a facilitating troponin site. Troponin sites are distributed over cellular space at every seven actin sites. Thus, for any actin site (i.e., $c = 1$ or 2), there must be one troponin site (i.e., a site in state 3 or 4) among $l1$, $l2$, $l3$, $r1$, $r2$, and $r3$. For a given troponin site (i.e., $c = 3$ or 4), its seventh-nearest neighbors, $l7$ and $r7$, must be troponin sites as well and could be in either state 3 or 4, respectively.

The neighborhood of a site in cellular space is defined as the set of its neighbors whose states have influence on the behavior of the site. The neighborhood of a actin site in our model consists of $r1$, $r2$, $r3$, $l1$, $l2$, and $l3$, and the neighborhood of a troponin site consists of $r1$, $r2$, $r3$, $r7$, $l1$, $l2$, $l3$, and $l7$ (see discussion in Appendix). The word "neighborhood-configuration" will refer to a certain arrangement of the neighborhood molecules in different states. For example, $r3 = 4$, $r2 = 1$, $r1 = 1$, $l1 = 1$, $l2 = 2$, and $l3 = 2$ represent one possible neighborhood-configuration of an actin site, and $r3 = 2$, $r2 = 2$, $l1 = 4$, $l2 = 2$, and $l3 = 1$ represent another.

c: the lattice site under consideration
l1:   the first left neighbor
l2:   the second left neighbor
l3:   the third left neighbor
l7:   the seventh left neighbor
r1:   the first right neighbor
r2:   the second right neighbor
r3:   the third right neighbor
r7:   the seventh right neighbor

FIGURE 4   Symbolic definition of neighbors in the neighborhood of a lattice site.

Because we assume that the whole process is essentially stochastic and driven by diffusion, the state transition rules are represented in the form of transition probabilities per unit time per molecule that correspond to the transition rate constants multiplied by the appropriate concentration value. A transition rule, in fact, is a function that specifies the state transition rate constant of an actin or a troponin site according to its neighborhood-configuration. In the simulation, all of the sites in the cellular space will use appropriate rules to update their states simultaneously at each time step according to their neighborhood-configurations.

There are two possible states for an actin and two possible states for a troponin in our model. The activation of an actin molecule (transition from state 1 to 2) is described by six transition rate constants, namely, $a_{12}^{(i)}$, $a_{12}^{(f)}$, b_{12}, c_{12}, d_{12}, and e_{12}, according to the neighborhood-configurations of the actin site. A graphic illustration of the transition rules related to these rate constants is shown

in Fig. 5. The deactivation rate constant (transition from state 2 to 1) of an actin is assumed to be independent of its neighborhood-configuration and is denoted by a_{21}. Similarly, the transition of a troponin site from inhibiting to facilitating (state 3 to 4) corresponds to the binding of calcium and is described by three state-transition constants, namely, a_{34}, b_{34}, and c_{34}, according to its neighborhood-configurations. Fig. 6 shows a graphic illustration of the transition rules related to these rate constants. The transition of a troponin site from facilitating to inhibiting (state 4 to 3) is assumed to be independent of its neighborhood-configuration and is denote by a_{43}. All state transition rules are summarized in Table 1. These rules are constructed based on the considerations of the structure of the thin filament and generally accepted assumptions about the interactions between actin, tropomyosin, troponin, and myosin head. Detailed discussion of the specification of these transition rules is presented in the Appendix.
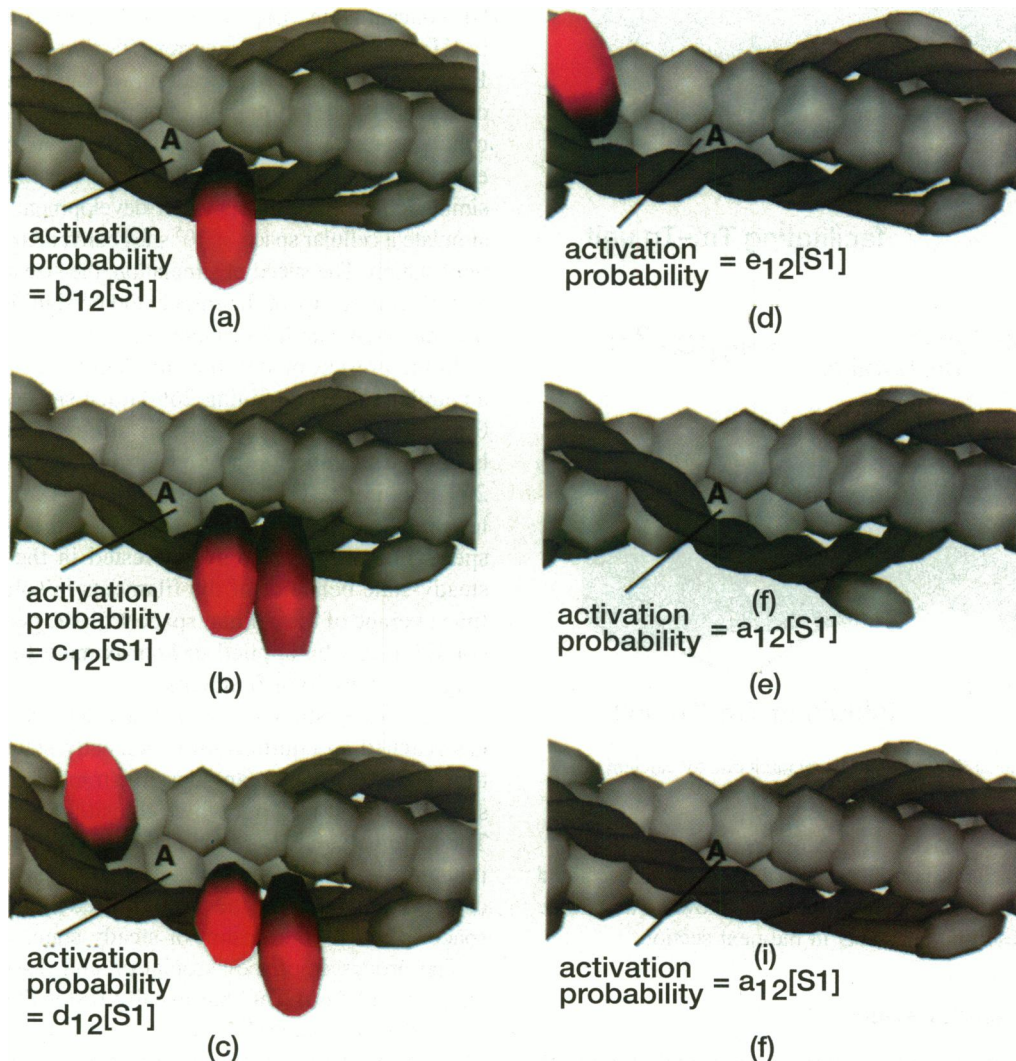

FIGURE 5 Graphical illustration of the activation rule for actin sites. Suppose we are considering the activation probability of the actin site labeled by "A" in a time step. The activation probability is different in six different cases determined by the states of proteins in the neighborhood of "A."

inhibiting Tm–Tn
transition probability $= b_{34}[Ca^{2+}]$

facilitating Tm–Tn unit

inhibiting Tm–Tn
transition probability $= c_{34}[Ca^{2+}]$

facilitating Tm–Tn unit

inhibiting Tm–Tn
transition probability $= a_{34}[Ca^{2+}]$
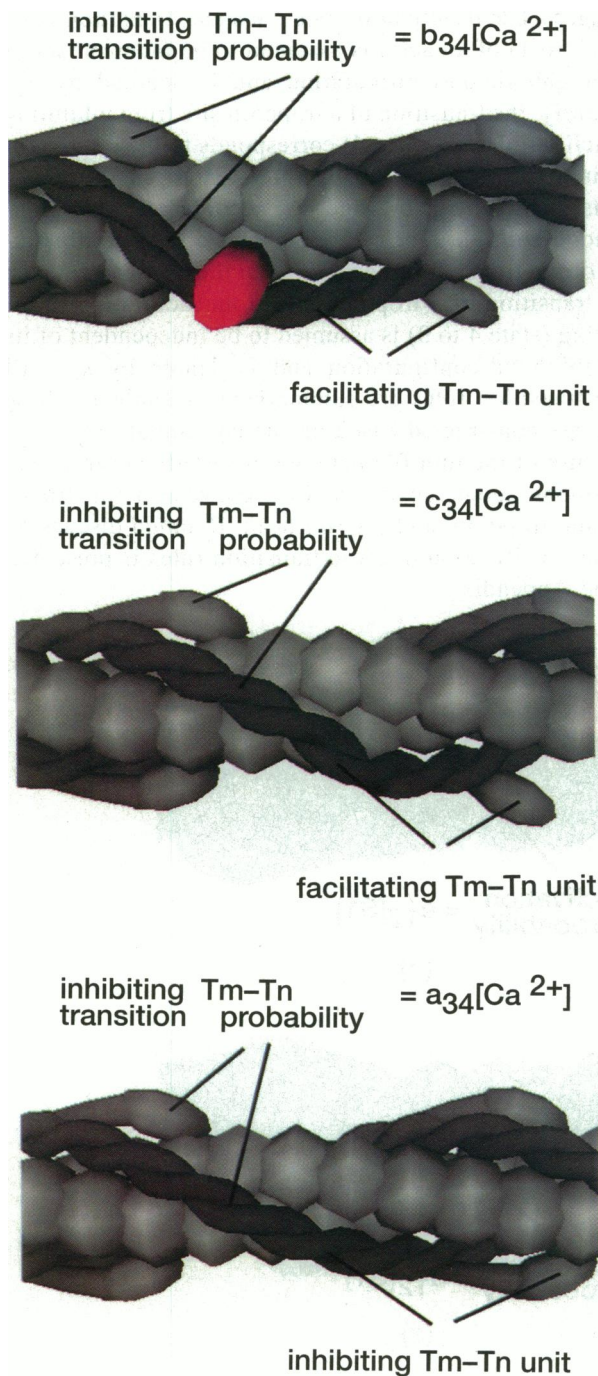

inhibiting Tm–Tn unit

FIGURE 6   Graphical illustration of the binding rule for calcium to TnC. There are three different situations.

The value of each rate constant in Table 1 has to be determined from experimental data. We will demonstrate how we determine the values of these rate constants in the next section.

Updating of cellular space

The simulation of the cellular automaton model starts with a particular initial configuration of the cellular space that consists of sites in states 1, 2, 3, or 4. Every site in the cellular

space can access the set of rules defined above. If, for example, at time t, a site finds that it is in state 1 (an inactive actin site), it will check its first-, second-, and third-nearest neighbors to see whether there are active neighbors and if it is under the influence of a facilitating or an inhibiting Tm-Tn unit. If, for example, its neighbors are not active and the corresponding Tm-Tn unit is in the inhibiting state, the site will then generate a random number and compare the random number with the probability $a_{12}^{(i)}$ [S1] to determine if it should transfer to state 2 or remain in state 1 at the next time step. After all state changes are decided, all sites in the cellular space update their states at the same time, which results a new generation of the cellular space at time $t + 1$. The number of sites in state i, denoted by $[s_i]$ ($i = 1, 2, 3,$ or 4) is counted at the end of each time step. If necessary, the concentration of S1 is updated at the end of each time step according to the equation

$$[S1] = [S1]_0 - \frac{[A][s_2]}{[s_1] + [s_2]}, \tag{2}$$

where [S1] is the current free S1 concentration, $[S1]_0$ is the total S1 concentration, [A] is the total actin concentration, and $[s_2]/([s_1] + [s_2])$ gives the current fraction of active actin sites. By repeating the above procedure, we can generate a sequence of cellular spaces at discrete time intervals. This sequence of cellular spaces, if it contains enough sites, can represent both the equilibrium and dynamic behavior of the thin filament. The simulation package that is under development will allow us to simulate a cellular space of 10^5 sites conveniently on a standard workstation. The speed of simulation, the size of cellular space, and the complexity of the rules could be significantly increased if a massively parallel machine is used.

In the present model, the simulations are conducted with a cellular space containing 266 lattice sites (numbered from 0 to 265). The cellular space is assumed to have periodic boundary conditions. In other words, we let sites 265, 264, 263, and 259 be l1, l2, l3, and l7 of site 0, respectively, and let sites 0, 1, 2, and 6 be r1, r2, r3, and r7 of site 265, respectively. If we are only interested in the equilibrium or steady-state behavior of the filaments in solution, the long-time average of the cellular space with the periodic boundary condition can be applied to approximate the ensemble average of many long filaments.

The next question is how we know when our cellular space has reached an equilibrium or a steady state. At any given time point, there are many possible transitions in the cellular space. We first find out which transition is the slowest one. Then, we calculate the time t_0 that is needed for the slowest transition to reach an equilibrium. Because t_0 is limiting, it can also be considered the time required for the entire cellular space to reach equilibrium or steady state.

The processes of the association and dissociation of calcium to and from TnC are usually faster than that of S1 to actin. The slowest transition is most likely to be the binding of S1 to an actin site that is inhibited by a nearby Tm-Tn unit. Indeed, as we will see in the next section, experimental data suggest that the activation rate constant of an inhibited actin

TABLE 1 Definition of kinetic constants and transition rules

Rate constant	Neighborhood-config.							Rate constant	Neighborhood-config.								
	c:	l3,	l2,	l1,	r1,	r2,	r3		c:	l7,	l3,	l2,	l1,	r1,	r2,	r3,	l7
b_{12}	1:	*,	1,	2,	1,	1,	*	b_{34}	3:	4,	2,	*,	*,	*,	*,	*,	*
	1:	*,	1,	1,	2,	1,	*		3:	4,	*,	2,	*,	*,	*,	*,	*
									3:	4,	*,	*,	2,	*,	*,	*,	*
c_{12}	1:	*,	*,	2,	1,	*,	*		3:	4,	*,	*,	*,	2,	*,	*,	*
	1:	*,	*,	1,	2,	*,	*		3:	4,	*,	*,	*,	*,	2,	*,	*
									3:	4,	*,	*,	*,	*,	*,	2,	*
d_{12}	1:	*,	*,	2,	2,	*,	*		3:	*,	2,	*,	*,	*,	*,	*,	4
									3:	*,	*,	2,	*,	*,	*,	*,	4
e_{12}	1:	*,	2,	1,	1,	*,	*		3:	*,	*,	*,	2,	*,	*,	*,	4
	1:	*,	*,	1,	1,	2,	*		3:	*,	*,	*,	*,	2,	*,	*,	4
									3:	*,	*,	*,	*,	*,	2,	*,	4
$a_{12}^{(l)}$	1:	4,	1,	1,	1,	1,	*		3:	*,	*,	*,	*,	*,	*,	2,	4
	1:	*,	4,	1,	1,	1,	*										
	1:	*,	1,	4,	1,	1,	*	c_{34}	3:	4,	1,	1,	1,	1,	1,	1,	*
	1:	*,	1,	1,	4,	1,	*		3:	*,	1,	1,	1,	1,	1,	1,	4
	1:	*,	1,	1,	1,	4,	*										
	1:	*,	1,	1,	1,	1,	4	a_{34}	3:	3,	*,	*,	*,	*,	*,	*,	3
$a_{12}^{(i)}$	1:	3,	1,	1,	1,	1,	*	a_{43}	4:	*,	*,	*,	*,	*,	*,	*,	*
	1:	*,	3,	1,	1,	1,	*										
	1:	*,	1,	3,	1,	1,	*										
	1:	*,	1,	1,	3,	1,	*										
	1:	*,	1,	1,	1,	3,	*										
	1:	*,	1,	1,	1,	1,	3										
a_{21}	2:	*,	*,	*,	*,	*,	*										

Here, "c" is the state of the site under consideration and "ln" and "rn" are the states of the nth left- and right-nearest-neighbor of the site under consideration, respectively. State 1 is an inactive actin; state 2, active actin; state 3, inhibiting Tm-Tn; and state 4, facilitating Tm-Tn. The symbol "*" indicates that the corresponding site in the neighborhood-configuration could be in either state 1 or 2 if it is an actin site and in either 3 or 4 if it is a troponin site.

$a_{12}^{(l)}$ is about 1.18 M^{-1} per time step, which is the slowest of all rate constants considered in this model. If we assume that all actin sites are inhibited by Tm-Tn units, the rate equation for the activation of actin sites would be

$$\frac{d[s_2]}{dt} = a_{12}^{(i)}[S1][s_1] - a_{21}[s_2] \qquad (3)$$

where $[S1]$ is the concentration of S1, and $[s_1]$ and $[s_2]$ are the concentrations of inactive and active actin, respectively. This equation is easily solved by changing variables; let $\Delta[s_1] = [s_1] - \overline{[s_1]}$, and $\Delta[s_2] = [s_2] - \overline{[s_2]}$, where the overbars denote equilibrium concentrations. Because $[s_1] + [s_2] = constant$, $\Delta[s_1] = -\Delta[s_2]$. Therefore, Eq. 3 becomes

$$\frac{d\Delta[s_2]}{dt} = -(a_{21} + a_{12}^{(i)}[S1])\Delta[s_2],$$

which has a solution

$$\Delta[s_2] = \Delta[s_2]_0 e^{-(a_{21} + a_{12}^{(i)}[S1])t}. \qquad (4)$$

At the equilibrium, $\Delta[s_2]$ should equal zero. Therefore, we can expect that an equilibrium is reached when

$$t \geq t_0 = 10 \times (a_{21} + a_{12}^{(i)}[S1])^{-1}. \qquad (5)$$

In the next section, we will show that a_{21} is about 10^{-2} step^{-1}, $a_{12}^{(i)}$ is about 10^1 M^{-1} step^{-1}, and the $[S1]$ used in the simulations is on the order of 10^{-7}–$^{-5}$ M. Therefore, $t_0 \simeq 1000$

time steps. Thus, we can consider that the cellular space is at the equilibrium or steady state after 1000 time steps.

COOPERATIVE BINDING OF S1 AND CALCIUM TO THE THIN FILAMENT

In this section, we will apply our model to previously obtained experimental data on the binding of calcium to the thin filament as published by Grabarek et al. (1983) and the data on binding of S1·ADP to actin sites obtained by Greene and Eisenberg (1980). We will show how each rate constant in our model is determined by these experimental data.

Model simulation

We simulate the dependence of S1 binding on free S1 concentration in the following manner. The initial states of lattice sites are assigned to reflect a specific experimental condition. We let the concentration of calcium remain fixed, and we let the concentration of S1 change over a certain range. For each $[S1]$ point, we update the cellular space for 10^3 time steps to reach equilibrium. After the equilibrium is reached, we start to count the number of sites in s_2 (the active actin sites) at each time step. The counting process continues for a period of 1.02×10^4 time steps, and the average number of s_2 ($[s_2]$)

is calculated at end of that period. Then, the time is reset to 0, the value of [$S1$] is increased by a certain amount, and another value of $\overline{[s_2]}$ can be obtained. By repeating the above process, we can get a set of $\overline{[s_2]}$ values and the corresponding [$S1$] values.

To compare our results to the experimental data, the simulations are conducted according to the calcium conditions as follows:

• *Low calcium concentration*: the initial configuration consists of lattice sites that are either in state 1 (inactive actin site) or in state 3 (inhibiting Tn). The state-3 sites are distributed along the cellular space at intervals of seven state-1 sites. The calcium concentration is set to a value [Ca^{2+}] = 10^{-8} M. The concentration of S1 then runs from 0 to 5 μM.

• *High calcium concentration*: the initial configuration is the same as in the above case. The calcium concentration is set to a value [Ca]$^{2+}$ = $10^{-4.5}$ M. The value [$S1$] ranges from 0 to 5 μM.

A similar procedure is used to simulate the binding of Ca^{2+} to the thin filament. The simulation is also conducted under two different conditions, matching those in the experiments:

• *In the absence of myosin*: the initial configuration consists of lattice sites that are either in state 1 or in state 3. The sites of state 3 are distributed along the cellular space at intervals of seven state-1 sites. The concentration of S1 is set to 0.0. The calcium concentration runs from pCa = 8.0 to 5.0. The number of lattice sites in state 4 (calcium bound state) is counted at every time step, and the average value $\overline{[s_4]}$ is calculated after 1.17×10^4 time steps.

• *In the presence of myosin*: the initial configuration is the same as that in the absence of myosin. The myosin concentration used in experiment was 1.65 μM (Grabarek et al., 1983), which is equivalent to [$S1$] = 3.3 μM because each myosin has two heads. The value [Ca^{2+}] ranges from 10^{-8} to 10^{-5} M. The value of $\overline{[s_4]}$ is obtained in the same way as that in the absence of myosin.

The simulations can be make to match the observed data quite well. Fig. 7 shows the simulation results of S1 binding compared with the experimental data of Green and Eisenberg (1980). Fig. 8 shows the comparison of simulation results of Ca^{2+} binding to the data of Grabarek et al. (1983).

Dissociation rate constant of calcium from thin filaments

We now show how the values of the transition rate constants in our model were derived from the experimental data. First, consider the dissociation rate constant of calcium release from the thin filament. It was reported that Ca^{2+} stays bound to TnC with a half-time of 2–3 ms (Johnson et al., 1979), which gives a value for the dissociation rate constant around 300 s^{-1}. This decreases to a value of 30 s^{-1} if TnC is part of a regulated thin filament (Potter and Gergely, 1975). The overall relaxation rate in skinned fibers, however, is even
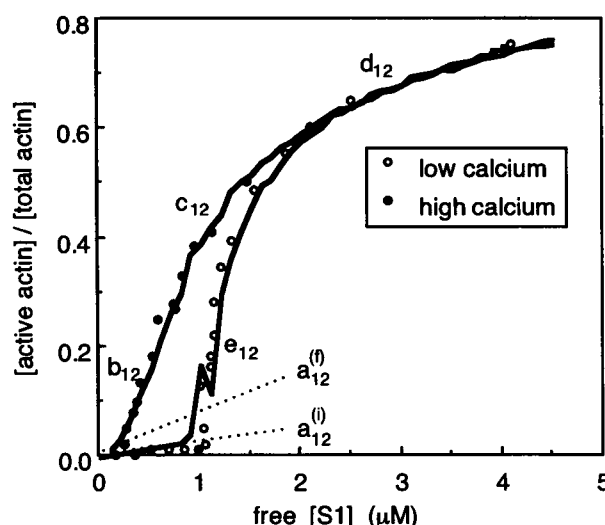

FIGURE 7   Comparison of the model simulation with the observed data of S1·ADP binding to the thin filament (Greene and Eisenberg, 1980). The total actin concentration of the data is 5.5 μM. The simulation is conducted with the same total actin concentration, and a calcium concentration of $10^{-4.5}$ M for the upper curve and $10^{-8.5}$ M for the lower curve. The initial direction of the upper curve is determined by activation rate constant $a_{12}^{(f)}$ and the initial direction of the lower curve is specified by activation rate constant $a_{12}^{(i)}$ as indicated by the dot lines in the figure. As [S1] increases, activation rate constants corresponding to other neighborhood protein configurations will take turns to dominate the control of the model behavior and, thus, can be individually determined by the corresponding data within appropriate [S1] ranges (see text for detail).

slower (on the order of 2 s^{-1}) (Moisescu, 1976). If we set the length of the time step in our model on the order of 1 to 30 ms, then we should let the rate constant, a_{43}, be on the order of 0.5 (time step)$^{-1}$.

Dissociation rate constant of S1 heads from actin

We now consider the the dissociation rate constant of·S1 detachment from actin filament, a_{21}. Because we are considering the strong binding of S1 to the thin filament in the presence of ADP (Greene and Eisenberg, 1980), the dissociation rate constant for S1 detachment should be much slower than that of Ca^{2+}. It was reported that the transition rate constant of A·M·ADP to M·ADP (here M stands for myosin S1) is on the order of 0.4 s^{-1} (Geeves, 1981). Thus, by comparison with the rate constant of dissociation of calcium from TnC, we let $a_{21} = a_{43}/50$.

Association rate constants of calcium for thin filaments in the absence of myosin

After setting up the dissociation rate constants, we then set the values for a_{34} and c_{34}, the association rate constants of calcium binding to the thin filament in the absence of myosin according to the experimental data of Grabarek et al. (1983). The rate constant a_{34} specifies the initial direction of the lower curve in Fig. 8 and should be determined mainly by the data at very low calcium concentration. The activation
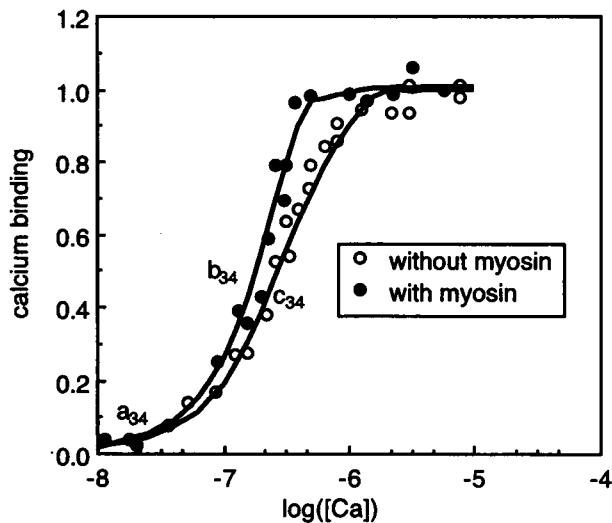
FIGURE 8 Comparison of the model simulation with the observed data of Ca^{2+} binding to the thin filament (Grabarek et al., 1983). The simulation was conducted under total actin concentration 4.7 μM, which is the same as that of the data, and the S1 concentration of 3.2 μM, which is twice as the myosin concentration 1.6 μM used in collecting the data. As the concentration of calcium increases, the association rate constants of calcium to TnC corresponding to various neighborhood protein configurations will take turns to dominate the control of model behavior, and can be determined by the data within appropriate pCa ranges (see text for detail).

rate constant c_{34} specifies the mid-range slope of the lower curve in Fig. 8 and is determined by the data at the relatively higher calcium concentration. The ratios $a_{34}/a_{43} = 8.70 \times 10^6$ and $c_{34}/a_{43} = 1.43 \times 10^7$ M^{-1} correspond to the affinity constants of the thin filament for Ca^{2+} at low and high $[Ca^{2+}]$, respectively.

Activation rate constants of actin sites

Now, we turn our attention to the activation rate constants of actin sites, $a_{12}^{(i)}$, $a_{12}^{(f)}$, b_{12}, c_{12}, d_{12}, and e_{12}. Activation of actin sites corresponds to the binding of S1. As we will see later, the effects of myosin on the binding of Ca^{2+} to the thin filament are significant only for middle range of $[Ca^{2+}]$. Under conditions of very high or very low calcium concentration, the association rate constant of Ca^{2+} binding to the thin filament in the presence of myosin is the same as that in the absence of myosin. Therefore, we can simulate the calcium binding by a_{34} and c_{34}, the association rate constants of Ca^{2+} binding to the thin filament in the absence of myosin, and determine the activation rate constants of actin sites under the conditions of high or low $[Ca^{2+}]$.

High calcium

We first consider the case of high calcium concentration and compare the model with the experimental data of S1 binding with high calcium concentration (Greene and Eisenberg, 1980). The activation rate constant $a_{12}^{(f)}$ corresponds to the neighborhood where the Tm-Tn unit is in a facilitating state and all actin sites are inactive (Table 1). Most actins are under

this situation when the fraction of active actin is very small (less than 0.05). Thus, the parameter $a_{12}^{(f)}$ should be responsible for the model behavior when the fraction of active actin is small or when [S1] is low, and can be determined by the data corresponding to [S1] < 0.2 μM (see Fig. 7). The association rate constant $a_{12}^{(f)}$ specifies the initial direction of the upper curve in Fig. 7.

If we raise the level of [S1] a little higher than 0.2 μM, more actin sites will be activated throughout the filament. At this point, many inactive actin sites begin to have isolated active neighbors. The activations of the actin sites that have isolated active neighbors are controlled by activation rate constant b_{12} (Fig. 5 a and Table 1). This type of activation will become dominant when the fraction of active actin is within 0.05 to 0.35 or when [S1] is between 0.2 and 0.8 μM in Fig. 7. The value of b_{12}, therefore, can be determined by the data within that [S1] range. The value of b_{12} specifies the slope of the upper curve in Fig. 7 within the [S1] range between 0.2 and 0.8 μM.

Increasing [S1] further, more inactive actin sites will be in a situation where they have two successive active neighbors (i.e., both the first- and the second-left-nearest neighbors or both the first- and the second-right-nearest neighbors are active). The activation of actin under this situation is controlled by rate constant c_{12} (Fig. 5 b and Table 1). The type of activation will become dominant when the fraction of active actin is between 0.35 and 0.5 or when [S1] is between 0.8 and 1.5 in Fig. 7. The value of c_{12} can be determined by the data in that [S1] range, and c_{12} specifies the slope of the upper curve in Fig. 7 within 0.8 < [S1] < 1.5 μM.

Increasing [S1] level beyond 1.5 μM, most inactive actin sites will have active neighbors on both sides (i.e., both left- and right-nearest neighbors and perhaps the second-nearest neighbors are active). The activation of these actin sites is controlled by the rate constant d_{12} (Fig. 5 c and Table 1), and the value of d_{12} can be determined by the data at the high end of [S1]. The association rate constant d_{12} specifies the slope of the upper curve in Fig. 7 at high S1 concentration.

The ratios $a_{12}^{(f)}/a_{21} = 10^5$, $b_{12}/a_{21} = 4.55 \times 10^6$, $c_{12}/a_{21} = 7.69 \times 10^5$, and $d_{12}/a_{21} = 5.56 \times 10^5$ M^{-1} correspond to the equilibrium binding constants of S1 to actin under the neighborhood-configurations specified in Table 1.

Low calcium

We now consider association of S1 to actin under conditions of low concentrations of calcium. The inhibiting behavior of the model at very low S1 concentration and in the absence of calcium is specified by the association rate constant $a_{12}^{(i)}$ (Fig. 5 f and Table 1). The rate constant $a_{12}^{(i)}$ specifies the initial direction of the lower curve in Fig. 7. The value of $a_{12}^{(i)}$ can be determined by the data with [S1] < 0.9 μM. The ratio $a_{12}^{(i)}/a_{21} = 1.28 \times 10^3$ M^{-1} gives the equilibrium binding constant of S1 to actin under inhibition Tm-Tn and low S1 concentration.

The slope of the lower curve in Fig. 7 around 1.0 μM is very sensitive to the association rate constant e_{12}. Thus, the

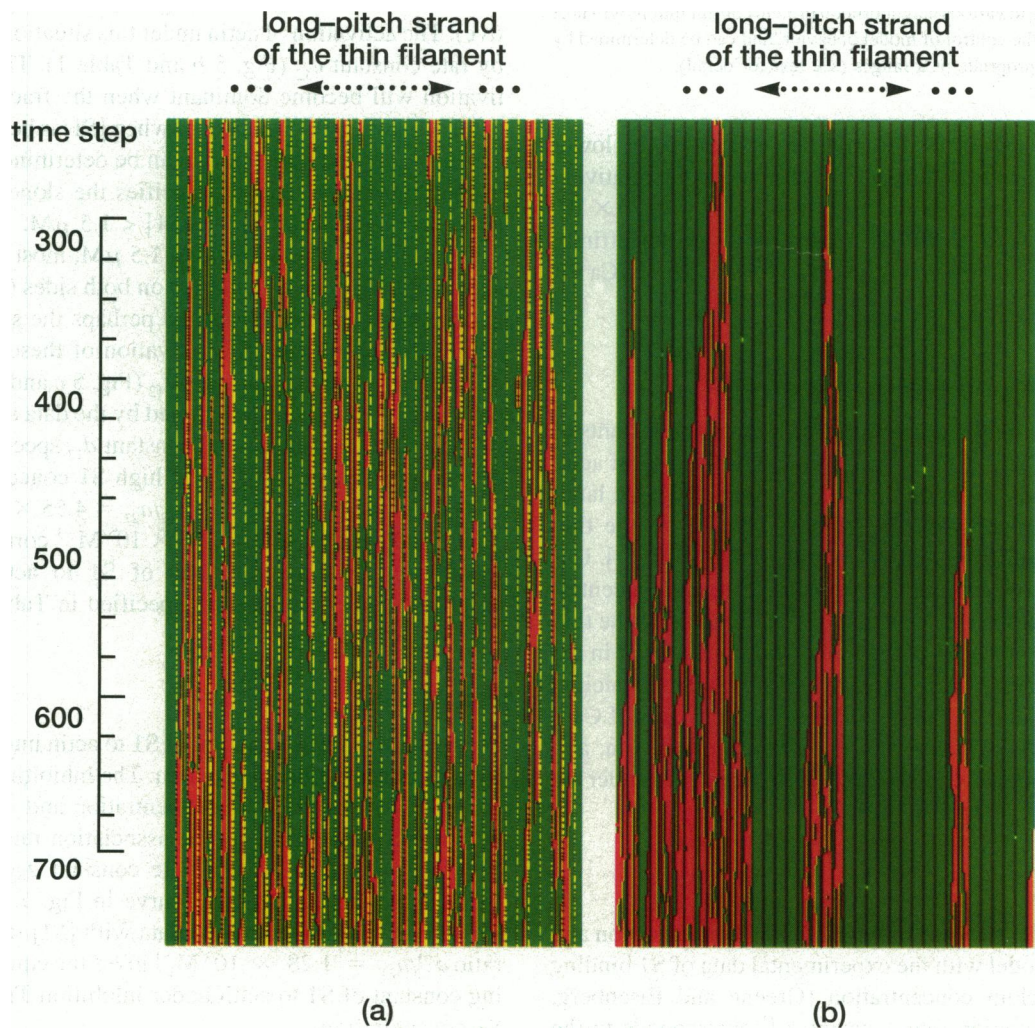**TABLE 2   The values of transition rate constants determined from experimental data**

Actin site transition rate constants		Troponin site transition rate constants	
b_{12}	$4.546 \times 10^4 M^{-1}step^{-1}$	b_{34}	$1.538 \times 10^7 M^{-1}step^{-1}$
c_{12}	$7.692 \times 10^3 M^{-1}step^{-1}$	c_{34}	$7.143 \times 10^6 M^{-1}step^{-1}$
d_{12}	$5.556 \times 10^3 M^{-1}step^{-1}$	a_{34}	$4.348 \times 10^6 M^{-1} step^{-1}$
e_{12}	$1.786 \times 10^3 M^{-1}step^{-1}$		
$a_{12}^{(f)}$	$1.000 \times 10^3 M^{-1}step^{-1}$		
$a_{12}^{(i)}$	$1.176 \times 10^1 M^{-1}step^{-1}$		
a_{21}	$1.00 \times 10^{-2}step^{-1}$	a_{43}	$5.00 \times 10^{-1}step^{-1}$

All notations used here are the same as those in Table 1.

value of e_{12} is determined by the data with [S1] between 0.8 and 1.2 μM. The association rate constant e_{12} results from the interaction between actin sites separated by a distance of one actin site (Fig. 5 d and Table 1). This "distant" interaction, however, does not play a significant role in the case of high calcium concentration.

Myosin effects on calcium binding

After the determination of the values of the association rate constants of S1, we can now try to set the value of b_{34}, the association rate constant for calcium binding to troponin on the thin filament in the presence of myosin. So far we have considered only the binding of individual S1 heads and not intact myosin. To apply our model to this data, we have to take the difference between S1 and myosin into consideration. First, each myosin has two heads. Thus, we should set [S1] to be twice the myosin concentration used in the experiment. Second, when one head of a myosin binds to one actin site, the second head, which is connected to the first, is always nearby. This situation is equivalent to a high S1 concentration around the actin site next to the first bound S1. We assume, therefore, that the binding of the second myosin head to an actin site will follow an effective S1 concentration of 20 μM, which gives a binding probability b_{12} [S1] $= 4.546 \times 10^4 \times 2 \times 10^{-5} \approx 0.9$ (step)$^{-1}$ for the second head. In other words, after one head

long–pitch strand of the thin filament

time step

300

400

500

600

700

(a)

long–pitch strand of the thin filament

(b)

FIGURE 9   The picture shows the dynamics of a portion of the cellular space from time step 256 to 765 corresponding to (a) the facilitating case, and (b) the inhibiting case in Fig. 7. The free S1 concentration is 1.0 μM in a and 4.0 μM in b.

of a myosin bind to an actin site, the other head has a 90% chance of binding to the next actin site within one time step. Under the above considerations, we determine the value b_{34} according to the data (Grabarek et al., 1983). The result is shown by the upper curve in Fig. 8.

Summary

Table 2 lists all of the values of the transition rate constants specified in Table 1. The absolute value of the rate constant depends on the length of the time step. The relative values between these rate constants, however, are quite important because they carry information about the interaction between molecules.

It can be observed in Fig. 7 that the critical phenomenon of switching of the thin filament with low [Ca^{2+}] occurs when free S1 concentration is around 1.0 μM. The detailed dynamic behavior of the thin filament in both cases of high and low calcium is shown in Fig. 9. Compare Fig. 9, a and b, and we can see that although the final fraction of the active actin is about the same, the spatial distribution and dynamics of S1 binding is quite different between facilitating and inhibiting situations. Strongly bound S1 tends to form much larger "clusters" in the inhibiting case and leads to an uneven distribution of activated actin sites along the thin filament. This clustering phenomenon is an example of a behavior of the system not explicitly included in the rules, but which arises from the interactions within the filaments. Of course, we do not yet know if it would correspond to the real system, but the clustering might be related to muscle dynamics and may be testable experimentally.

PREDICTING THE ACTO-S1 ATPASE ACTIVITY

It should be possible to extend the model to include not only binding of myosin and calcium, but also ATPase activity. The acto-S1 ATPase is thought to take place at a certain point in the cycle of strong binding of S1 to actin and release. An active actin site thus contributes only to the ATPase once throughout the cycle of its activation. A reasonable assumption is that every actin site has a contribution to the acto-S1 ATPase when it enters the active state. Therefore, instead of counting the the number of total active actin sites, we should count as ATPase events the number of actin sites that just enter the active state at the end of each time step.

The ATPase data (Lehrer and Morris, 1982) were collected when ATP concentration was sufficient to saturate the system, whereas the S1 binding data (Greene and Eisenberg, 1980) were obtained under the condition where ADP was excessive. The dominant deactivation process for actin under high ATP concentration (the condition of ATPase data) (Lehrer and Morris, 1982) involves the transition from A·M·D to A·M·T or M·T (Fig. 10). The transition from A·M·D to M·D occurs very rarely during hydrolysis of ATP by acto-S1 (Cooke, 1986). The average deactivation rate constant is between 7 to 12 s^{-1} for these two processes (Rosenfeld and Taylor, 1987). The dominant
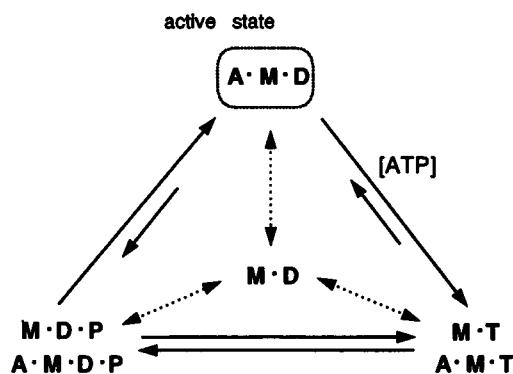

active state

FIGURE 10 The simplified steps in the hydrolysis of ATP by actomyosin. Here M represents a myosin head (S1); A, actin; T, ATP; D, ADP; and P, inorganic phosphate. During the steady-state cycle of ATP hydrolysis by acto-S1, A·M·T and M·T as well as A·M·D·P and M·D·P are in rapid equilibrium. The transitions marked by dotted lines occur very rarely during hydrolysis of ATP by acto-S1. Arrows of unequal length connecting states indicate that this transition is favored in the direction of the longer arrow.

deactivation process of actin under high ADP concentration (the condition of S1·ADP binding data) (Greene and Eisenberg, 1980) is from A·M·D to M·D in Fig. 10, and the rate constant is about 0.4 s^{-1} (Geeves, 1981). Therefore, we should increase the deactivation rate constant, a_{21}, 20 to 30 times for the simulation of ATPase activity to match the experimental conditions.

It can be seen from Fig. 10 that, in presence of ATP, inactive actin sites are distributed in both A·M·T and A·M·D·P. In principle, actin sites may be activated directly from either of these two species. However, under condition of high ATP concentration, dominant activation is from A·M·D·P, which is in a rapid equilibrium with M·D·P, to A·M·D. During this process, A·M·D·P releases P_i and converts to strong binding to actin. The strong binding process should be essentially the same as that of M·D to A·M·D (Fig. 10). Therefore, we use the same activation rate constants obtained from the analysis of S1·ADP binding data (Greene and Eisenberg, 1980) in last section to simulate ATPase activity.

Fig. 10 also shows that, in the presence of ATP, S1 heads that are not in the strong binding configuration (considered as free S1 in our model) could be in several different forms, namely, A·M·T, M·T, M·D, A·M·D·P, and M·D·P. The binding of ATP to actomyosin causes a rapid dissociation of myosin with a rate constant of 5000 s^{-1} (Geeves, 1981). However, the dissociation is not complete, leading to the conclusion that A·M·T and M·T are in rapid equilibrium (Stein et al., 1981, 1979; White and Taylor, 1976). Upon addition of ATP, the initial degree of protein association, measured for skeletal acto-S1 by turbidity, was the same as that at steady state, so the equilibrium between states A·M·T and M·T and states A·M·D·P and M·D·P must be similar (White and Taylor, 1976). The hydrolysis by the protein complex, i.e., the transition from A·M·T to A·M·D·P occurs with a rate similar to hydrolysis on myosin alone

(Stein et al., 1981; Mornet et al., 1981). Thus, the process occurs rapidly compared with the overall cycle time and is not rate-limiting here. It is safe, therefore, to keep the assumption that the activation of actin is proportional to the total concentration of S1 that is not in the strong binding configuration. This concentration of S1 can be calculated by subtracting the active actin concentration from the total S1 concentration.

If we let q be the hydrolysis produced by one μM actin site upon activation, the total acto-S1 ATPase activity of our model can be calculated as

$$\text{ATPase} = \frac{q[A](\text{number of actin sites entering active state})}{(\text{total number of actin sites})}, \quad (6)$$

where $[A]$ is the total actin concentration, and in the simulation, we let $q = 1.4 \times 10^{-2}$. Notice that the turnover value q is not taken from the literature and, therefore, can be treated as a prediction of our model and tested experimentally.

The acto-S1 ATPase activity can be simulated in a similar manner to S1 binding. The simulation of acto-S1 ATPase is conducted as closely as possible to the experimental conditions (Lehrer and Morris, 1982) as follows:

• *Actin + Tn + Tm − Ca²⁺*: the initial configuration consists of lattice sites that are either in state 1 (inactive actin site) or in state 3 (inhibiting Tm-Tn unit). The state-3 sites are distributed along the cellular space every seven lattice sites. The calcium concentration is set to a value of $10^{-7.5}$ M. The concentration of S1 then runs from 0 to 10 μM.

• *Actin + Tn + Tm + Ca²⁺*: The initial configuration is the same as in the above case. The calcium concentration is set to a value of $10^{-4.5}$ M. The value [S1] ranges from 0 to 10 μM.

The simulation results for acto-S1 ATPase (Fig. 11) compare well with the experimental data published by Lehrer and Morris (1982). Except for the deactivation rate constant of actin which, according to the literature, is 20 to 30 times faster in the presence of ATP, all values of the transition rate constants are the same as those in Table 2. Thus, the model can simultaneously fit key aspects of the equilibrium binding of myosin and calcium and steady-state ATPase data.

CONCLUSION AND DISCUSSION

The interaction between strongly bound S1 heads

In our model, we assume that the transition rate constant of an actin site is a function of its neighborhood-configuration. The assumption defines an alternative perspective from which information can be extracted from the existing experimental data. For example, by comparing the model behavior with the S1 binding data observed by Greene and Eisenberg (1980), we found a fivefold difference between transition rate constants b_{12} and c_{12}, which correspond to two different neighborhood-configurations (Table 2). The transition rate constant b_{12} corresponds to the activation of an
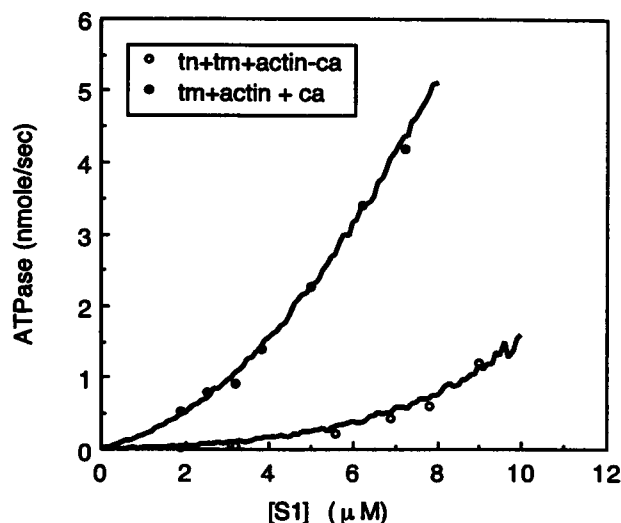

FIGURE 11 Comparison of the model prediction with experimental data on ATPase activity (Lehrer and Morris, 1982). Curves are the model simulations, which are plotted against the corresponding data in two different cases, respectively. The data are collected with a total actin concentration of 3.2 μM. The same total actin concentration is used in the simulations.

actin site when one of its nearest neighbors is active and the successively second-nearest neighbor is not active (Fig. 5 *a*, Table 1, see Appendix for detailed discussion). The transition rate constant c_{12} is for the activation of an actin site when one of its nearest neighbor is active and the successively second-nearest neighbor is also active (Fig. 5 *b*, Table 1, see Appendix for detailed discussion). The difference between the two rate constants implies that there are, indeed, interactions between successively bound S1 heads.

Initially, an S1 head has to push tropomyosin to achieve strong binding to an actin site. The probability of this initial binding is either $a_{12}^{(f)}$ or $a_{12}^{(i)}$ depending on the state of the corresponding Tm-Tn unit. After the binding of the first S1, a second S1 could bind to the actin site next to the first S1 with a much higher probability, which is specified by b_{12}. It seems that a third S1 should be able to bind to the inactive actin site next to either the first S1 or the second S1 with the same probability as that of the second S1, i.e., c_{12} should equal to b_{12} because the tropomyosin position around the actin site should be the same in both cases. Therefore, it was at first a surprise to us that parameters b_{12} and c_{12} are different by a factor of 5. However, the model could not fit the experimental data if we assumed that the two parameters are the same, i.e., if we do not distinguish the two situations (see Fig. 5, *a* and *b*).

One possible explanation for the difference in the binding probability of the second and third S1 heads is that a strongly bound head behaves differently when it is alone and when there is another strongly bound head next to it. The binding of the third S1, therefore, requires extra free energy to overcome the interference caused by the interaction between the first and second S1. Thus, it seems that S1 heads tend to bind in pairs, even though they are not covalently connected as myosin or heavy meromyosin.

Some of these effects might play a critical role in the muscle function. For example, in the last section we have to assume a large binding probability of the second myosin head to explain satisfactorily the myosin effect on the calcium binding.

Interaction between neighboring Tm-Tn units

Evidence shows that only the two Ca^{2+}-specific sites on TnC are directly involved in the regulation of muscle contraction (Grabarek et al., 1983; Johnson et al., 1979). Although the binding of Ca^{2+} to these sites on isolated TnC or the ternary troponin complex exhibits no cooperativity (Grabarek et al., 1983), measurements of the relationship between the Ca^{2+} concentration and its binding to the thin filament yield a steep curve demonstrating cooperative metal binding (Grabarek et al., 1983). The cooperativity is further increased to give a Hill coefficient greater than 2.4 in the presence of myosin. The Ca^{2+} dependence of various physiological parameters such as myofibrillar ATPase activity and tension development in fibers shows an even higher Hill coefficient (>4). The cooperative metal binding, therefore, is not accounted for simply by the cooperativity of the calcium binding sites on TnC. Experiments show that upon the binding of Ca^{2+} to TnC, a series of conformational changes are propagated through tropomyosin-troponin complex to allow the formation of interactions between myosin and actin (Leavis, 1984). It is also reported that the strong binding of myosin heads to actin alters the structure of TnC through the thin filament protein interactions (Zot and Potter, 1989). It seems more natural, therefore, to treat the continuous tropomyosin-troponin complex as an integrated functional unit, and to consider the cooperative binding of Ca^{2+} to thin filaments a result of the interaction between the neighboring Tm-Tn units. Thus, the individual calcium binding sites on TnC can be assumed in our model to bind calcium-independently at all times, which is consistent with the observation in the case of isolated molecules.

Our cellular automaton model has been constructed based on the above considerations, and the performance of the model seems to be supportive of the assumptions. In our model, parameter a_{34} represents the binding rate constant of Ca^{2+}, parameter c_{34} characterizes the interaction between neighboring Tm-Tn units, and parameter b_{34} corresponds to the interaction of Tm-Tn units in the presence of strongly bound S1 heads. We had specified another parameter, a'_{34} to represent the binding rate constant of Ca^{2+} in the presence of myosin. However, to fit the data, we find that $a'_{34} = a_{34}$. This implies that attachment of myosin heads to actin does not alter the basic affinity of Tm-Tn unit for Ca^{2+}; rather, it strengthens the interaction between a facilitating Tm-Tn unit and an inhibiting Tm-Tn unit. As a result, the myosin effects on the calcium binding become insignificant under a condition of very low $[Ca^{2+}]$, where most Tm-Tn units are in inhibiting state, or very high $[Ca^{2+}]$, where most Tm-Tn units are in facilitating state.

It is notable that the interaction between bound myosin heads discussed in the previous section also plays a significant role in affecting Ca^{2+} binding to the thin filament. Without assuming a large binding probability of the second myosin head, we cannot obtain a good fit of the model simulation to the experimental data. Also, with this model, we cannot observe the even greater effect on the binding of Ca^{2+} to the thin filament caused by ATP reported in Grabarek et al. (1983). The reason is that we are not considering the effects of weak binding of myosin heads in the current model. Evidence shows that both weak and strong binding produce some conformational changes in the TnC (Zot and Potter, 1989). These effects will be explored in subsequent models.

The interaction of the Tm-Tn unit with actin has been shown to lower the affinity of the regulatory sites of TnC for Ca^{2+} (Zot and Potter, 1987). If we also assume that additional interactions are present in intact fibers and that the affinity is further lowered in muscle fiber, then the even higher cooperative metal binding in fibers could easily be explained and qualitatively illustrated by our model. First, we reduce the value of the parameter a_{34}, which corresponds to the association rate constant of calcium binding to the thin filament, and let all other parameters in the model remain the same. Then, we assign a constant value to [S1] to imitate the effective concentration of myosin heads in isometric fibers and let the calcium concentration change over a range from pCa value 7 to 5. The simulation result is shown in Fig. 12. The "tension" in our model simulation corresponds to the normalized average number of actin sites that leave the active state (resume the weak binding) at each time step. As shown in Fig. 12, the very steep observed pCa/tension relationship is r·edicted by the model. This extrapolation of our model illustrates its usefulness in testing cause and effect relationships of different basic assumptions.

Evidence also shows that the shape and position of the pCa/tension curve depend on a variety of solution parameters
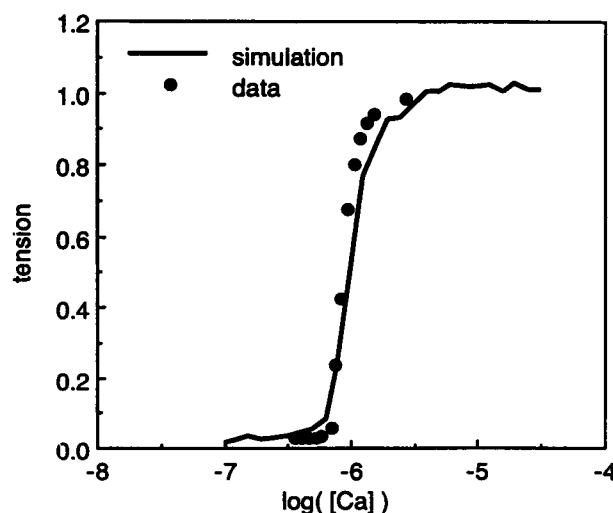

FIGURE 12 The pCa/tension relationship simulated by the model in comparison with the data in fiber (7).

(Brandt et al., 1982; Donaldson and Kerrick, 1975). Many of the solution parameters might cause changes in the various transition rate constants in our model. The overall effect of the changes in behavior of the individual components can be quantitatively evaluated by our model. For example, the change in the calcium affinity of a mutant TnC can alter the shape of pCa/tension relationship. This effect can be simulated by varying parameter a_{34} in our model over a certain range of values (Fig. 13). Note that changing the association rate constant (and, hence, the equilibrium constant) does not simply shift the pCa/tension curve but changes the steepness as well. Similarly, we can also examine the individual and the combined effects of other transition processes on the pCa/tension curve. Because the current model does not include geometrical factors presented in fibers, further simulation and discussion will be carried out in subsequent versions. We believe models such as these will be crucial in explaining effects of site-specific mutants in the study of contracting events.

Dynamic aspects of the thin filament in fibers

In molecular biology or physiology, we are concerned with the movement and alteration of the molecules during their interaction with other molecules in a supermacromolecular system. However, because of the complexity in the nature of the problem, most of the theoretical models must concentrate on the equilibrium or steady state rather than the dynamical processes. Cellular automata, however, are intrinsically dynamical. Thus, the cellular automaton model proposed here can be extended to account for the observed dynamics of thin filaments even in intact muscle fibers. In the following, we will use our current model to simulate qualitatively the dynamical behavior of muscle thin filaments in fibers. Detailed study of the phenomena in fibers, however, requires further elaboration of the current model.
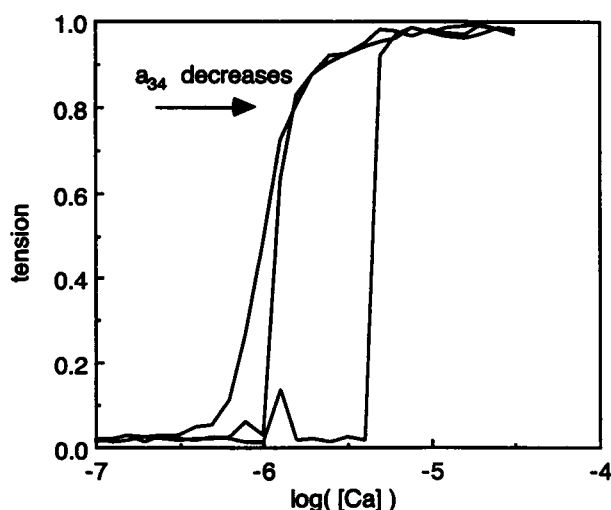
The recent development of synchrotron radiation has been able to provide x rays of much higher intensity and has made the study of dynamic structural changes in muscle on the millisecond time scale possible (Huxley and Faruqi, 1983; Ebashi et al., 1991). The dynamic x-ray diffraction during muscle contraction reveals that there are intensity changes in the layer lines corresponding to the thin filaments during contraction. The comparison of time courses of intensity changes of the equatorial x-ray reflections with the Ca^{2+} transient from sarcoplasmic reticulum using a single frog skeletal muscle fiber (Konishi et al., 1991; Ebashi et al., 1991) shows a time delay between the peaks of calcium transient and the intensity changes of the 1,0 and 1,1 reflections (Fig. 14 a). The increase of the intensity changes run almost parallel to the time course of lag-corrected aequorin light signal during stimulation, while returning to the resting value with a significant delay behind the aequorin light during relaxation.

If we assume that the x-ray intensity changes correspond to change of the population of strongly bound S1 to the thin filament, we can also use our current model to run a qualitative dynamic simulation. In the micromolar $[Ca^{2+}]$ range, the aequorin light emission is proportional to $[Ca^{2+}]^{2.5}$ (Allen et al., 1977). In the simulation, the aequorin light signal is mimicked by three exponential functions, and $[Ca^{2+}]$ is calculated based on the light signal. Both number of active actin sites and $[Ca^{2+}]$ are recorded at each time step. The values of all transition rate constants used for this simulation are identical to those used for the pCa/tension simulation (Fig.12). The simulated time courses of the relative changes of the total number of active actin sites and the calcium concentration in our model are shown in Fig. 14 b. The match of the model to the data is again quite good. The development of cellular space corresponding to the simulated muscle contraction is shown in Fig. 15. The activation is seen to occur in patches, with some parts of the thin filament more active than others. Implications of this stochastic "patchiness" are not clear, but it may be important to consider when discussing overall aspects of force development.

Experimental data from x-ray diffraction shows that it usually takes about 0.05 to 0.23 s for the relative intensity change of thin filaments to reach its maximum from the resting level. By comparing our simulation result with the data (Ebashi et al., 1991; Huxley et al., 1982), it can be seen that the time step in our model is from 1 to 10 ms, which is consistent with the step-length assumption we have made when assigning the value for the calcium dissociation rate constant.

General remarks

The cellular automaton model we proposed in this paper is the simplest version that we could construct and still observe the behavior seen in key experiments. The states of actin sites admittedly represent a simplification of the cross-bridge cycle; detailed kinetic steps of the cross-bridge cycle have been ignored for now. More than two states of actin would be needed to distinguish, for example, weak binding from
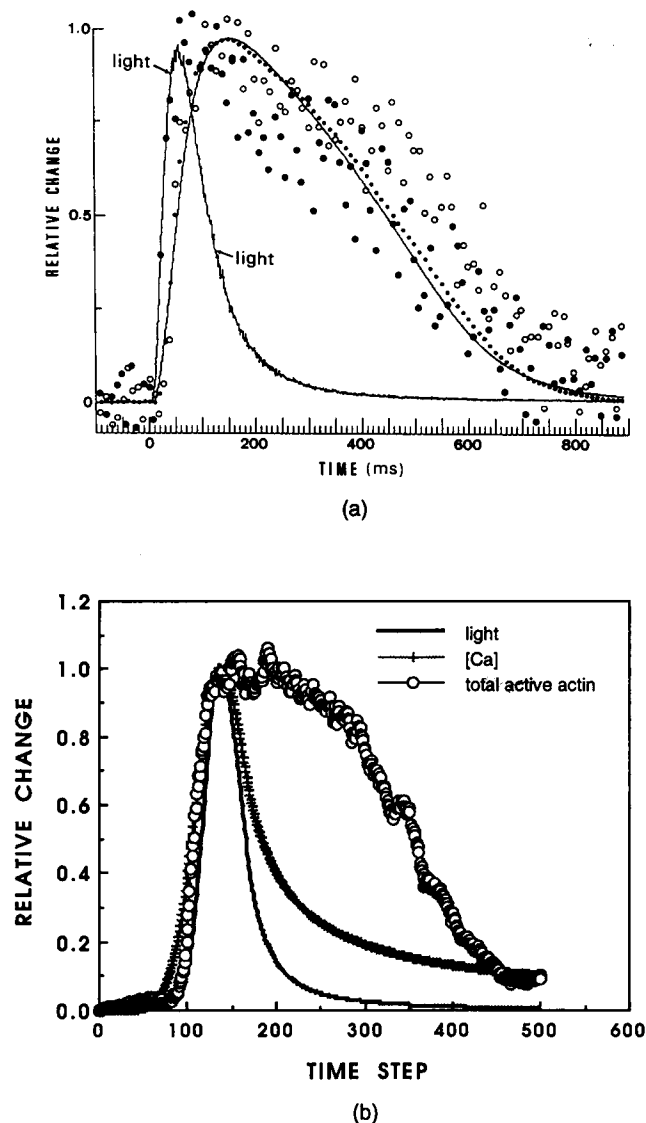

FIGURE 13 The simulated effect of calcium affinity (corresponding to the parameter a_{34}) on the pCa/tension curve.

(a)

TIME STEP

(b)

FIGURE 14   (a) The time courses of the 1, 0 (○) and 1,1 (●) equatorial x-ray reflections and $[Ca^{2+}]$ transient as monitored by aequorin light (labeled by "light") during an isometric twitch (reprinted from Konishi et al., 1990). (b) The time courses of the relative changes of the total number of active actin sites and the calcium concentration in our model simulation. For the modeling, calcium concentration is based on the assumption that aequorin light emission is proportional to $[Ca^{2+}]^{2.5}$. The simulation generally matches the experimental data seen in a and allows us to determine that one time step in our model is about 2 ms. The peak of $[Ca^{2+}]$ transient appears earlier than the peak of the change of total number of active actin sites by 30–60 time steps. The time delay between the return of the total number of active actin sites to the resting value during the relaxation and the change of $[Ca^{2+}]$ is also reproduced by the model.
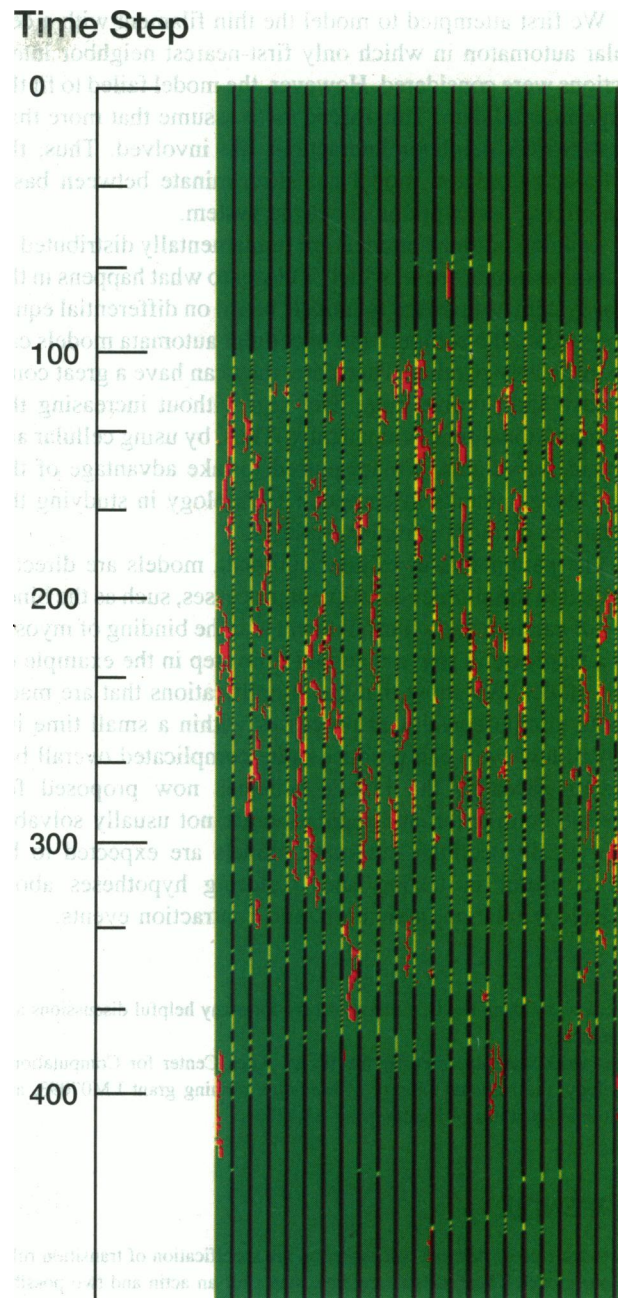

FIGURE 15   The time evolution of a portion of the cellular space corresponding to the simulated muscle contraction in Fig. 14. The red patches correspond to active actin sites, and the yellow sites correspond to "facilitating" troponin-tropomyosin units.

unbound states. Further elaboration of our model to account for observations in real muscle fibers is also possible, but beyond the scope of this study. The additional states seem unnecessary for fitting the model to the experimental data that we are considering here.

We utilized the idea in this paper that the strong binding of S1 to actin sites is blocked by tropomyosin and that an S1 head has to move tropomyosin to make a strong interaction with actin. This idea, however, is only used for the conve-

nience in description and in graphic illustration. The model does not distinguish between these details of the mechanism. It is possible that an actin site under the influence of tropomyosin has a greater affinity for myosin than that in the absence of tropomyosin. The main point of model is that the interaction among tropomyosin, troponin, myosin, and actin can change the affinity of an actin site for myosin. As a result, different configurations of the these proteins in the neighborhood of an actin site set up different activation rate constants for that site.

We first attempted to model the thin filament with a cellular automaton in which only first-nearest neighbor interactions were considered. However, the model failed to fit the experimental data. This forced us to assume that more than first-nearest neighbor interactions are involved. Thus, the cellular automaton model can discriminate between basic underlying assumptions about the system.

Cellular automata models are fundamentally distributed in a computational sense, which is closer to what happens in the real system as opposed to models based on differential equations. Also, the computation of cellular automata models can be massively parallel. Therefore, they can have a great complexity and involve huge data sets without increasing the computational time dramatically. Thus, by using cellular automata paradigms, we are poised to take advantage of the new developments in computer technology in studying the behavior of more complex systems.

The parameters in cellular automata models are directly related to the simpler constituent processes, such as the binding of calcium to the thin filament and the binding of myosin to a single actin site at a certain time step in the example of our model. We show that the simplifications that are made about simple constituent processes within a small time interval, however, can produce quite complicated overall behavior. Because the kinetic schemes now proposed for muscle contraction and regulation are not usually solvable analytically, cellular automata models are expected to be more useful in testing and exploring hypotheses about muscle regulation, activation, and contraction events.

APPENDIX

Here we present detailed discussion on the specification of transition rules in our model. There are two possible states for an actin and two possible states for a troponin-tropomyosin unit. We discuss the state-transition rule for each of these states individually.

Inactive actin sites

The activation of an inactive actin site corresponds to the transition of state 1 to 2 in our model, and also to the transition of a green lattice site at time t to a red lattice site at time $t + 1$ in cellular space. We denote this state-transition as

$$s_1 \xrightarrow{k_{12}} s_2,$$

where k_{12} is the transition probability for a given actin site in a unit time, or in this case, the probability of activation of a given actin site in a unit time. Because the activation of an actin site corresponds to the binding of myosin S1 in a particular way, the transition probability of s_1 to s_2 in a unit time should be proportional to the S1 concentration ([$S1$]), i.e.,

$$k_{12} = a_{12}[S1],$$

where a_{12} is a constant coefficient with a unit of $M^{-1} s^{-1}$, which corresponds to the first-order association rate constant of S1 binding to actin. Let ΔG be the total free energy change during the S1 binding, and

$$\Delta G = \Delta G_0 + \Delta G_p,$$

where ΔG_p is the positive free energy required to move the tropomyosin during the S1 binding and ΔG_0 is the function of the free energy change caused by attachment of myosin. Because

$$k_{12}/k_{21} \propto e^{-(\Delta G_0 + \Delta G_p)/kT},$$

where k_{21} is the reverse transition probability of s_1 to s_2, and k_{21} is assumed to be independent of S1 and actin concentrations (see discussion below), we could have the following relation between the association rate constant a_{12} and the free energy change ΔG_p:

$$a_{12} \propto e^{-(\Delta G_0 + \Delta G_p)/kT}.$$

The free energy ΔG_p could be modified by two possible sources: (i) the state of the corresponding Tm-Tn unit, and (ii) the states of the neighboring actin sites. The other portion of the free energy change ΔG_0 is assumed not to be affected.

The largest amount of ΔG_p is needed to move the tropomyosin molecule when the corresponding Tm-Tn unit is in the inhibiting state. A lesser (perhaps even negative) amount of ΔG_p is required to do the same, when the corresponding Tm-Tn unit is in the facilitating state. Thus, the state of the Tm-Tn unit alone sets up two different situations, namely, facilitating influence and inhibiting influences.

The actin sites that are subject to the influence of a Tm-Tn unit are those that are covered by the Tm-Tn unit, i.e., the actin sites that are located within a distance of three lattice sites from the corresponding troponin molecule. Thus, the above mentioned two situations can be specified by:

- Facilitating influence: r1, r2, r3, l1, l2 or l3 = 4.
- Inhibiting influence: r1, r2, r3, l1, l2, or l3 = 3.

Different situations corresponds to different free energy ΔG_p and, therefore, different association rate constant a_{12}. The probability of activation can be written as

$$k_{12} = \begin{cases} a_{12}^{(f)}[S1] & \text{if (r1, r2, r3, l1, l2, or l3 = 4)} \\ a_{12}^{(i)}[S1] & \text{if (r1, r2, r3, l1, l2, or l3 = 3),} \end{cases} \quad (7)$$

where $a_{12}^{(f)}$ and $a_{12}^{(i)}$ are constant coefficients with a unit of $M^{-1} s^{-1}$ and correspond to the first-order association rate constants of S1 binding to actin under facilitating and inhibiting situation, respectively.

After an S1 head is bound to an actin site, the tropomyosin has been moved significantly around that site such that S1 can be bound to its neighboring sites without much free energy expenditure on the tropomyosin movement regardless whether the Tm-Tn unit is in facilitating or inhibiting state. In other words, if there are active neighbors, an actin site has a much greater chance to be activated and the activation is not influenced by the state of the corresponding Tm-Tn unit. Meanwhile, however, the bound S1 also interferes with the S1 binding activity of the neighboring sites. Overcoming this interference will cause free energy expenditure. The interference can become significant and reduce the chance of activation of an actin site if the site has too many active neighbors. The above consideration can be implemented by the following rule:

$$k_{12} = \begin{cases} b_{12}[S1] & \text{if (r1 = 2 and r2, l1, l2 $\neq$ 2) or} \\ & \text{if (l1 = 2 and l2, r1, r2 $\neq$ 2)} \\ c_{12}[S1] & \text{if (r1 = 2 and l1 $\neq$ 2) or} \\ & \text{if (l1 = 2 and r1 $\neq$ 2)} \\ d_{12}[S1] & \text{if (r1 = 2 and l1 = 2)} \\ e_{12}[S1] & \text{if (r2 = 2 or l2 = 2),} \end{cases} \quad (8)$$

where b_{12}, c_{12}, d_{12}, and e_{12} are constant coefficients with a unit of $M^{-1} s^{-1}$ and correspond to the first-order association rate constants of S1 binding to an actin site under different neighborhood-configurations.

Combine Eq. 7 and Eq. 8, and we have the complete transition rule for state 1 as follows:

$$k_{12} = \begin{cases} b_{12}[S1] & \text{if } (r1 = 2 \text{ and } r2, l1, l2 \neq 2) \text{ or} \\ & \text{if } (l1 = 2 \text{ and } l2, r1, r2 \neq 2) \\ c_{12}[S1] & \text{if } (r1 = 2 \text{ and } l1 \neq 2) \text{ or} \\ & \text{if } (l1 = 2 \text{ and } r1 \neq 2) \\ d_{12}[S1] & \text{if } (r1 = 2 \text{ and } l1 = 2) \\ e_{12}[S1] & \text{if } (r2 = 2 \text{ or } l2 = 2) \\ a_{12}^{(f)}[S1] & \text{if } (r1, r2, r3, l1, l2, \text{ or } l3 = 4) \\ a_{12}^{(i)}[S1] & \text{if } (r1, r2, r3, l1, l2, \text{ or } l3 = 3). \end{cases} \quad (9)$$

Fig. 5 provides a graphic illustration of an example of the above transition rule. The rule simply implies that there are six different neighborhood-configurations that result in different association rate constants of S1 binding to actin. Notice that by specifying the above rule for an actin site, we do not exclude the possibility that actin sites also directly interact with each other in the absence of tropomyosin. In fact, the conclusion of our model does show the existence of a direct interaction between two active actin sites. The rule will also be summarized in a tabular form of transition rates as a function of neighborhood-configurations at the end of this section.

Active actin sites

An activated actin site, of course, can become inactive. This corresponds to the reversible transition of state 2 to 1, and to the transition of a red lattice site at time t to a green lattice site at time $t + 1$ in cellular space. We denote the transition as

$$s_2 \xrightarrow{k_{21}} s_1,$$

where k_{21} is the transition probability for a given active actin site in a unit time. We assume that the deactivation of an actin site is a first-order process and that the deactivation probability is always a constant. Therefore, the transition rule for the active actin site is

$$k_{21} = a_{21}, \quad (10)$$

where a_{21} has a unit of s^{-1} and corresponds to the dissociation rate constant of S1 from actin.

Inhibiting troponin molecules

The transition of a troponin molecule from the inhibiting state to the facilitating state corresponds to the transition of state 3 to state 4 in our model, and also to the transition of a black lattice site at time t a yellow lattice site at time $t + 1$ in cellular space. The transition is denoted as

$$s_3 \xrightarrow{k_{34}} s_4,$$

where k_{34} is the transition probability of a given troponin in a unit time.

It is believed that the binding of two calcium ions to troponin triggers the conformational change of Tm-Tn unit and causes the release of ATPase inhibition. Experiments (Grabarek et al., 1983) also shows that only two low affinity calcium binding sites on troponin C (TnC) are responsible to the calcium regulation, and no cooperativity in these two sites were observed in free peptide as well as in ternary complex of TnC. We assume, therefore, that two Ca^{2+} binding sites are independent of each other, and the transition probability of a given inhibiting troponin molecule in a unit time is proportional to the calcium concentration, i.e.,

$$k_{34} = a_{34}[Ca^{2+}],$$

where $[Ca^{2+}]$ is calcium concentration and a_{34} is a constant coefficient.

In our model, we consider that the state-change of a troponin molecule is equivalent to the conformational change of the entire Tm-Tn unit. The current state of a Tm-Tn unit should have an influence on the state transition

of its neighboring Tm-Tn units. We assume, therefore, that the transition probability of an inhibiting troponin increases when either one or both of its nearest neighboring Tm-Tn units are in a facilitating state, and increases further if there are active actin sites in its neighborhood. Because two nearest neighboring troponin molecules are separated by a distance of seven lattice sites in cellular space, we have the following rule:

$$k_{34} = \begin{cases} b_{34}[Ca^{2+}] & \text{if } (r7, \text{ or } l7 = 4) \text{ and} \\ & \text{if } (r1, r2, r3, l1, l2, \text{ or } l3 = 2) \\ c_{34}[Ca^{2+}] & \text{if } (r7 \text{ or } l7 = 4) \text{ and} \\ & \text{if } (r1, r2, r3, l1, l2, \text{ and } l3 = 1) \\ a_{34}[Ca^{2+}] & \text{if } (r7 \text{ and } l7 = 3) \text{ and} \\ & \text{if } (r1, r2, r3, l1, l2, \text{ and } l3 = 1 \text{ or } 2), \end{cases} \quad (11)$$

where the coefficients a_{34}, b_{34}, and c_{34} represent the first-order overall association rate constants of $[Ca^{2+}]$ binding to TnC under different situations. Fig. 6 provides a graphic illustration of an example of the above transition rule. The rule specifies three different association rate constants of Ca^{2+} binding to a given inhibiting Tm-Tn unit under three different neighborhood-configurations. We could assume more possible neighborhood-configurations; however, the three configurations listed above form the minimum set of rules that is required to explain the experimental data (see discussion).

Facilitating troponin molecules

The transition of a troponin molecule from the facilitating state to the inhibiting state corresponds to the transition of state 4 to state 3, and to the transition of a yellow lattice site at time t to a black lattice site at time $t + 1$ in cellular space. The transition is denoted as

$$s_4 \xrightarrow{k_{43}} s_3.$$

where k_{43} is the transition probability per unit time.

For simplicity, we assume that the facilitating conformation of a Tm-Tn unit transfers back into the inhibiting conformation with a constant probability in a unit time period, i.e.,

$$k_{43} = a_{43}, \quad (12)$$

where a_{43} has a unit of s^{-1} and corresponds to the overall dissociation rate constant of $[Ca^{2+}]$ release from the thin filament.

Summary

All of the rules we have specified correspond to a function that determines the transition rate constant of any given site according to its neighborhood-configuration, and can also be represented in tabular form as shown in Table 1.

REFERENCES

Allen, D. G., J. R. Blinks, and F. G. Prendergast. 1977. Aequorin luminescence: relation of light emission to calcium concentration—a calcium-independent component. *Science.* 195:996–998.

Brandt, P. W., R. N. Cox, and M. Kawai. 1980. Can the binding of Ca^{2+} to two regulatory sites on troponin C determine the steep pCa/tension relationship of skeletal muscle? *Proc. Natl. Acad. Sci. USA.* 77: 4717–4720.

Brandt, P. W., R. N. Cox, M. Kawai, and T. Robinson. 1982. Regulation of tension in skinned muscle fibers. *J. Gen. Physiol.* 79:997–1016.

Brookshear J. G. 1989. Theory of Computation. Benjamin/Cummings Publishing Company, Inc., New York. 21 pp.

Chalovich, J. 1992. Actin mediated regulation of muscle-contraction. *J. Pharmacol. Exp. Ther.* 55:95–148.

Cooke, R. 1986. The mechanism of muscle contraction. *CRC Crit. Rev. Biochem.* 21:53–118.

DasGupta, G., and E. Reisler. 1992. Actomyosin interactions in the presence of ATP and the N-terminal segment of actin. *Biochemistry.* 31: 1836–1841.

Donaldson, S. K., and W. Kerrick. 1975. Characterization of the effects of Mg^{2+} on Ca^{2+} and Sr^{2+}-activated tension generation of skinned skeletal muscle fibers. *J. Gen. Physiol.* 66:427–444.

Ebashi, S., M. Koch, and E. Ruberstein. 1991. Handbook on Synchrotron Radiation. Vol.4. Elsevier, New York.

Geeves, M. A. 1981. The dynamics of actin and myosin association and the crossbridge model of muscle contraction. *Biochem. J.* 274:1–14.

Grabarek, Z., J. Grabarek, P. C. Leaves, and J. Gergely. 1983. Cooperative binding to the Ca^{2+}-specific sites of troponin C in regulated actin and actomyosin. *J. Biol. Chem.* 258:14098–14102.

Greene, L. E., and E. Eisenberg. 1980. Cooperative binding of myosin subfragment-1 to the actin-troponin-tropomyosin complex. *Proc. Natl. Acad. Sci. USA.* 77:2616–2620.

Hibberd, M. G., and D. R. Trentham. 1986. Relationships between chemical and mechanical events during muscle contraction. *Annu. Rev. Biophys. Biochem.* 15:119–161.

Hill, T. L. 1983. Two elementary models for the regulation of skeletal muscle contraction by calcium. *Biophys. J.* 44:383–396.

Hill, T. L., E. Eisenberg, and L. Greene. 1980. Theoretical model for the cooperative equilibrium binding of myosin subfragment 1 to the actin-troponin-tropomyosin complex. *Proc. Natl. Acad. Sci. USA.* 77: 3186–3190.

Huxley, H. E., and A. R. Faruqi. 1983. Time-resolved X-ray diffraction studies on vertebrate striated muscle. *Annu. Rev. Biophys. Bioeng.* 12: 381–417.

Huxley, H. E., A. R. Faruqi, and M. Kress. 1982. Time-resolved X-ray diffraction studies of the myosin layer-line reflections during muscle contraction. *J. Mol. Biol.* 158:637–684.

Johnson, J. D., S. C. Charlton, and J. D. Potter. 1979. A fluorescence stopped flow analysis of Ca^{2+} exchange with troponin-C. *J. Biol. Chem.* 254: 3497–3502.

Kauffman, S. A. 1969. Metabolic stability and epigenesis in randomly constructed genetic nets. *J. Theor. Biol.* 22:437–467.

Konishi, M., K. Wakabayashi, S. Kurihara, H. Higuchi, N. Onodera, Y. Umazume, H. Tanaka, T. Hamanaka, and Y. Amemiya. 1991. Time-resolved synchrotron X-ray diffraction studies of a single frog skeletal muscle fiber. *Biophys. Chem.* 39:287–297.

Leavis, P. C. 1984. Thin filament proteins and thin filament-linked regulation of vertebrate muscle contraction. *CRC Crit. Rev. Biochem.* 16: 235–305.

Lehrer, S. S., and E. P. Morris. 1982. Dual effects of tropomyosin and troponin-tropomyosin on actomyosin subfragment 1 ATPase. *J. Biol. Chem.* 14:8073–8080.

Lymn, R. W., and E. W. Taylor. 1971. Mechanism of adenosine triphosphate hydrolysis of actomyosin. *Biochemistry.* 10:4617–4624.

McKillop, D. F. A., and M. A. Geeves. 1991. Regulation of the acto-myosin subfragment 1 interaction by troponin/tropomyosin. *Biochem. J.* 279: 711–718.

Moisescu, D. G. 1976. Kinetics of reaction in calcium-activated skinned muscle fibers. *Nature.* 262:610–613.

Mornet, D., R. Betrand, P. Pantel, E. Audemard, and R. Kassab. 1981. Structure of the actin-myosin interface. *Nature.* 292:301.

Phillips, Jr., G. N., J. P. Fillers, and C. Cohen. 1986. Tropomyosin crystal structure and muscle regulation. *J. Mol. Biol.* 111–131.

Potter, J. D., and J. Gergely. 1975. The calcium and magnesium binding sites on troponin and their role in the regulation of myofibrillar adenosine triphosphatase. *J. Biol. Chem.* 250:4628–4633.

Rayment, I., and H. M. Holden. 1993. Myosin subfragment-1: structure and function of a molecular motor. *Curr. Opin. Struct. Biol.* 3:944–952.

Rosenfeld, S. S., and E. W. Taylor. 1987. The mechanism of regulation of actomyosin subfragment 1 ATPase. *J. Biol. Chem.* 262:9984–9993.

Stein, L. A., P. B. Chock, and E. Eisenberg. 1981. Mechanism of the actomyosin ATPase: effect of actin on the ATP hydrolysis step. *Proc. Natl. Acad. Sci. USA.* 78:1346–1350.

Stein, L. A., P. B. Chock, and E. Eisenberg. 1979. Mechanism of actomyosin adenosine triphosphatase. Evidence that adenosine 5'-triphosphate hydrolysis can occur without dissociation of the actomyosin complex. *Biochemistry.* 18:3985–3909.

Tobacman, L. S., and R. S. Adelstein. 1986. Mechanism of regulation of cardiac actin-myosin subfragment 1 by troponin-tropomyosin. *Biochemistry.* 25:798–802.

White, H. D., and E. W. Taylor. 1976. Energetics and mechanism of actomyosin adenosine triphosphate. *Biochemistry.* 15:5818–5826.

Williams, Jr., D. L., L. E. Greene, and E. Eisenberg. 1988. Cooperative turning on of myosin subfragment 1 adenosinetriphosphatase activity by the troponin-tropomyosin-actin complex. *Biochemistry.* 27: 6987–6993.

Wolfram, S. 1984. Cellular automata as models of complexity. *Nature.* 311:419.

Zot, A. S., and J. D. Potter. 1989. Reciprocal coupling between troponin C and myosin crossbridge attachment. *Biochemistry.* 28:6751–6756.

Zot, H. G., and J. D. Potter. 1987. Calcium binding and fluorescence measurements of dansylaziridine-labelled troponin C in reconstituted thin filaments. *J. Muscle Res. Cell Motil.* 8:428–436.